Where is PELE? Pervasive localization using wearable and handheld devices

Luis Henrik John
Delft University of Technology
Delft, The Netherlands
l.h.john@student.tudelft.nl

Chayan Sarkar
TCS Research
Kolkata, India
sarkar.chayan@tcs.com

R. Venkatesha Prasad
Delft University of Technology
Delft, The Netherlands
r.r.venkateshaprasad@tudelft.nl

ABSTRACT

Smartphones or in general handhelds commonly used for indoor localization purposes are not a viable option in places where people do not carry them all the time – for example, home and office. Alternatively, wearable devices can partially solve this problem but have many limitations with respect to power supply, processing capability, and availability of sensors. These issues prevent the adoption of many common handheld localization solutions. In this work, we present **PE**rvasive **L**ocalization **E**ngine (PELE), a distributed localization system that uses wearable and handheld jointly to address the above drawbacks. Using only magnetometer, accelerometer, and Bluetooth radio, localization is performed by means of a particle filter. In addition, a dynamic handoff mechanism is presented, which uses the wearable only when it is necessary, thus reducing energy consumption on the wearable without affecting the desired localization accuracy. Evaluating the system with ten participants, we achieve a localization accuracy of 90.31 % in an indoor environment spanning about 320 m^2.

CCS CONCEPTS

• **General and reference** → *Performance*; • **Computer systems organization** → *Embedded software*;

KEYWORDS

Indoor localization, wearable, joint localization, handoff, pervasive

ACM Reference Format:
Luis Henrik John, Chayan Sarkar, and R. Venkatesha Prasad. 2018. Where is PELE? Pervasive localization using wearable and handheld devices. In *Proceedings of Advances in IoT Architecture and Systems, Toronto, Canada, June 2017 (AIoTAS'17),* 8 pages.

1 INTRODUCTION

Personal indoor localization has been considered an important constituent of pervasive IoT applications, as people spend approximately 90 % of their time in indoor environments [25]. Existing indoor localization systems generally localizes a handheld (e.g., smartphone, tablet, etc.), which in turn localizes the user [9]. These devices provide data from a variety of sensors and have sufficiently large processing capability. Though such solutions are highly appropriate for most of the public indoor spaces such as shopping malls or airports, they are less applicable for home and office environments, where users may not carry such a device all the time; they remain static for long duration. Users within such non-public indoor spaces are the target audience of this work.

Use cases. As location information is one of the most important contextual information for many IoT applications, continuously localizing a user is an important step forward. For example, Sarkar *et al.* [20] proposed a room-level indoor lighting and heating control system that depends on locations of the occupants. Similarly, location information of a person is utilized to track the activities remotely in the elderly care system [21].

Motivation. Recently, inexpensive wearable devices such as smartwatches, fitness trackers, body-worn cameras, head-mounted displays, smart garment, etc., have become increasingly accessible. Of all the wearables, currently, only smartwatches are comparable with handheld in terms of processing capabilities and sensors. However, out of 274 M wearable devices sold worldwide in 2016 (estimated), only about 18% are smartwatches [24]. Thus, handheld-based indoor localization algorithms or solutions cannot be easily adapted for most of the affordable and less complex wearables. However, they are able to track and measure various human activities continuously, as they are envisioned to be worn on the body all the time (or at least either of them is worn throughout the day). This provides the opportunity to utilize wearable devices for ubiquitous indoor localization, where the wearables may guarantee completeness of sampled sensor data, while the handheld can be responsible for more demanding processing tasks.

Challenges. A number of challenges need to be tackled in order to achieve a pervasive localization using wearable and handheld. Firstly, the radio communication between handheld and wearable, and sensor sampling rate should not exhaust the devices' energy. As a continuous sampling of the sensor is highly inefficient from the energy point of view, they have to be sampled at a proper rate. Secondly, the lack of sensors and/or radio interfaces on the wearables, due to their smaller form factor, limits the use of existing localization methods. Finally, devices and their components are developed by the various manufacturer. Modeling these components for a common goal without any human intervention is a challenge.

Contributions. We propose the **PE**rvasive **L**ocalization **E**ngine (PELE) that jointly uses a wearable and a handheld. Using the integrated accelerometer and magnetometer, the wearable is localized relative to the handheld's absolute location, which is assumed to be acquired by one of the common handheld-based localization techniques [9, 22]. The location of the user is determined by employing a particle that uses sensor data from the wearable. The specific contributions of this work are as follows.

- We present a practical, non-intrusive, infrastructure-free localization solution for location-based IoT services. To the best of our knowledge, this is the first work to propose a joint localization system using a pair of wearable and handheld devices.

AIoTAS'17, June 2017, Toronto, Canada

- To overcome the limitations in processing capacity of a wearable, computational tasks are delegated to a handheld without incurring significant energy consumption.
- To strike a balance between location accuracy and energy efficiency, the system uses a dynamic hand-off mechanism to start and stop the localization process on the wearable.

Based on our evaluation with ten participants, on an area of about 320 m^2 comprising of ten rooms, PELE achieves a localization accuracy of 90.31 %. In the next section, we provide a brief survey of various indoor localization techniques. Section 3 and 4 present overview and detailed description of the system, respectively. The system evaluation is presented in Section 5 before concluding the article in Section 6.

2 RELATED WORK

Lymberopoulos *et al.* [12] broadly categorize the indoor localization techniques into two classes – (i) infrastructure-based, and (ii) infrastructure-free. Finger printing technique is one of the popular infrastructure-based localization technique (Fig. 1a). It consists of two phases. In the offline phase, a radio map of fingerprints is generated, associating ambient radio signals with physical locations. During the online working phase, a device that observes the ambiance is able to collect real-time fingerprint and compare it to the radio map using pattern matching algorithms in order to estimate its location. For example, a system of localizing patients in a hospital environment is proposed in [2], where RFID tags and readers are used for finger printing. Similarly, SEAMLOC [17] uses WLAN signals for finger printing. Though finger printing can provide a good location accuracy, it requires a number of transmitters in the vicinity. Moreover, it is prone to changes in the environment and relies strongly on unaltered conditions between offline and online phase.

Geometric properties of triangles offer an alternative infrastructure-based localization approach. Triangulation measures the bearing relative to beacons placed in known locations [5]. Such direction based techniques make use of the Angle of Arrival (AoA) or the Angle of Departure (AoD) to define arcs, whose intersection estimates users' location. As neither wearable nor handheld holds an antenna array, direct angle measurement is not possible. Of course, when localization using triangulation is envisioned with a single handheld beacon, high location ambiguity is expected.

Another infrastructure based localization technique is proximity sensing, where detecting spatial closeness of objects provides relative location (Fig. 1c). A device that is detected by an antenna can be considered collocated with that antenna. When dense antenna grids are used, it is considered to be collocated with the one receiving the strongest signal [11]. Similar to fingerprinting, the method is rendered unusable by having the beacon from a single transmitter.

Since the infrastructure based techniques often involve expensive deployments in terms of time and money, it renders unsuitable for many applications. As a result, infrastructure-free systems are widely used as well. Integration of inertial measurement units (IMUs), commonly comprised of accelerometer, gyroscope and magnetometer, enable measurement of body-specific forces, angular rates and magnetic orientation of subjects. Using the infrastructure-free pedestrian dead-reckoning (PDR) methodology (shown in Fig. 1d), the absolute location of a user can be determined by computing stride length, walking direction and integrating steps [8, 22]. By nature, PDR systems suffer from cumulative error introduced by the environment, but also due to noisy sensed data. However, activities such as ascending and descending stairs, using the elevator or standing at some usual points are used to recognize landmarks and increase localization precision.

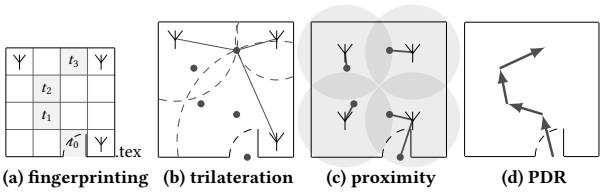

(a) fingerprinting (b) trilateration (c) proximity (d) PDR

Figure 1: Common indoor localization techniques.

Nowadays hybrid systems are more common and made up of at least two of the methodologies explained earlier. For example, Ubicarse [10] uses WLAN based triangulation, and the sensor data from accelerometer, magnetometer and gyroscope is used to estimate the antenna position. Furthermore, the camera of the mobile device is used for geo-tagging objects. Similarly, Wang *et al.* [23] employed an unsupervised learning to extract unique sensor signatures from landmarks, and dead-reckoning based schemes track location in between landmarks. Using landmark based recalibration, the system continues to improve localization accuracy over time. The approach does not require a specialized infrastructure, except the ground plan of the building. However, it is rather prone to changes in the ambiance.

Though the hybrid solutions provide an increasingly accurate indoor positioning, complexity of the systems increases by crowd sourcing approaches and sampling of a multitude of sensors. Infrastructure is required for fingerprinting, geometric methods and proximity sensing. On the contrary, there is limited attention given to the widely available and affordable fitness trackers, which make up a majority of wearables. These devices are generally not advanced enough for complex hybrid solutions. We opt to use geometric methods with a single beacon and eliminate location ambiguity with a low accuracy dead-reckoning approach.

3 SYSTEM OVERVIEW

In this section, the assumptions and design goals that lead to the system design are discussed. Furthermore, a conceptual overview of the system is provided.

3.1 Initial assumptions

The localization process of PELE works in two different modes – (i) *standalone*, and (ii) *joint*. In the *standalone* mode, only the handheld device is used for localization, whereas in the *joint* mode, both the handheld and the wearable devices are used. Since there exists a number of solutions that provide sufficiently accurate indoor localization using a handheld device, no new technique is developed for the standalone mode. Without loss of generality, a particle filter-based dead-reckoning technique is adopted for the *standalone mode*, as used in [16]. Our major contribution lies in the joint localization

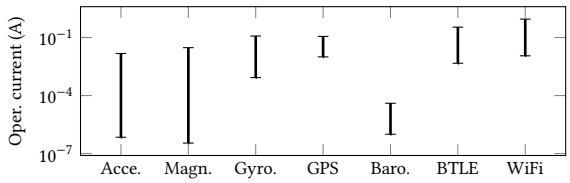

Figure 2: Comparison of sensor energy consumption.

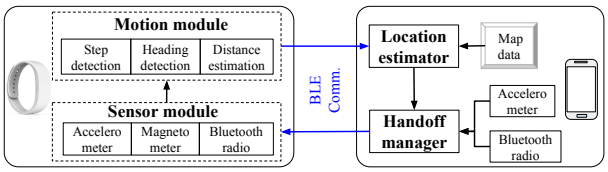

Figure 3: System overview of PELE.

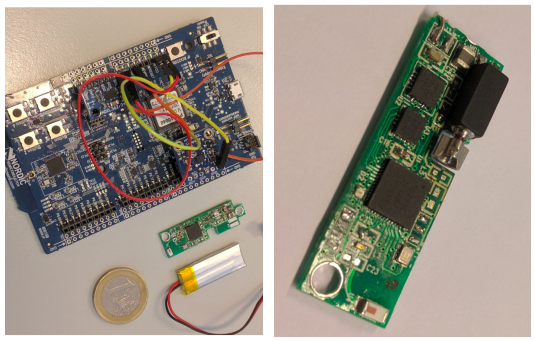

(a) Development board with PELE board is next to it. **(b) Designed PELE wearable.**

Figure 4: Hardware configuration of the wearable.

system, thus rest of the article describes and evaluates the system only for the *joint mode*.

We assume an infrastructure free localization requirement with the floor plan known beforehand. For most of the indoor living places, room-level accuracy is sufficient. However, room size may vary significantly. As Bluetooth is the only radio interface on most wearables, it is used to communicate with the handheld.

Choice of Sensors. Accelerometer, gyroscope, and magnetometer are used in combination for step detection and heading estimation. As most wearables do not feature all the three sensors (except few smartwatches), we aim to choose sensors that provide the basic functionality and draw lower power. Due to the wide range of operating currents of various sensor components, a direct comparison of energy consumption is difficult. Based on our survey of two major electrical component distributors [3, 6], we concluded that a magnetometer can provide more efficient operation than a gyroscope while acquiring heading information (see Fig. 2). That is because a gyroscope requires continuous sampling to estimate heading direction. Additionally, integration of the gyroscope data is computationally intensive, and causes a cumulative bias error that is often difficult to rectify. Note that a magnetometer can also be biased by magnetic interferences in indoor environments. However, this error may be diminished by combining a Bluetooth RSS based distance measurement along with the dead-reckoning. Thus, we consider only an accelerometer and a magnetometer to be present.

3.2 Design goals

The crux of PELE is to share the load of sensing and processing between the handheld and wearable in order to localize a person continuously. This amounts to the following two design goals. **First**, as wearables have limited battery capacity, the usage of sensors has to be optimized towards energy efficiency without losing the required location accuracy. Thus, sensor sampling needs to be triggered only when it is required. **Second**, due to their restricted memory and processing capability, sensor data processing cannot be performed entirely by most of the commercial low-end wearables. Thus, some of the computational tasks need to be delegated to the handheld. However, keeping the energy constraint in mind, communication between the two devices also need to be kept at minimal.

3.3 Architecture

Fig. 3 depicts a pictorial overview of PELE's architecture. The distributed model is inspired by our previous works [18, 19]. By default, the localization process is executed on the handheld device in the *standalone* mode. The system triggers the *joint* mode by automatically detecting when the user transfers without carrying the handheld. As soon as the person starts roaming with the handheld again, the process is switched back to the *standalone* mode and any localization-related activity on the wearable is stopped. In the following, we briefly introduce the major building blocks of PELE.

Handoff manager. Handoff manager runs on the handheld and selects a suitable localization mode while ensuring a sufficient localization accuracy. Its goal is to reduce energy consumption by avoiding unnecessary sampling of the sensors on both the devices.

Sensor module. The sensor module resides on the wearable, and it turns on and off the sensors on the device on the directive of the handoff manager. It also optimizes the sampling rate for the sensors to achieve a balance between energy efficiency and data granularity, which in turn also optimizes the communication between the wearable and the handheld.

Motion module. The motion module resides on the wearable. By processing the raw sensor data, it estimates three pieces of information about users' movement, i.e., step event detection, heading direction, and distance from the stationary handheld device.

Location estimator. The location estimator resides on the handheld. It receives the motion model outputs from the wearable over the Bluetooth connection. It integrates this information with the map data using a particle filter-based dead-reckoning approach. In addition using the distance information, the integration bias is supposed to be minimized.

3.4 Hardware configuration

Commercially available wearables generally do not provide an API that would allow for extensive reconfiguration. Therefore, a wearable, PELE, was designed based on state of the art hardware components. The system on chip nRF52 serves as Bluetooth enabled microcontroller. In addition an affordable accelerometer as well as

magnetometer was added. Figure 4 shows the development board of the microcontroller with mounted sensors and the wearable board after assembly. The cost of PELE is around $15. The form factor is 3 cm by 0.1 cm and is 0.5 cm thick.

4 PELE ON THE FIELD

In this section, the details of the building blocks are provided (Fig. 3). It is described how they work in synergy to achieve pervasive localization.

4.1 Handoff manager

The handoff manager is responsible for switching between the mutually exclusive *standalone* and *joint* localization modes (Fig. 5). The goal is to avoid sampling and data processing on wearable and handheld simultaneously and thus preserve energy. In general, handoff may take place when the user leaves behind the handheld and moves around. A trivial solution would be to trigger the *joint* mode as soon as the accelerometer data in the handheld suggests that the device is stationary. Similarly, switching back to the *standalone* mode is done, when the handheld becomes mobile again. However, this solution may lead to unnecessary switching between the two modes and hence superfluous sensor usage on the wearable. For example, when the user keeps the handheld on a desk and sits next to it, the unnecessary handoff would cause energy drain on the wearable.

Since we are aiming at room-level accuracy, there is no need to handoff unless the user moves out of the room in which the handheld is located (referred to as *handheld* room). However, if the handoff takes place only after the user moves out of the room, it takes a long time to determine the location of the user, especially in the case when there are multiple adjacent rooms to the *handheld room*. Given our particle filter based localization technique, we found that correct and expeditious particle convergence can be guaranteed, when the handoff to *joint* mode takes place before transferring to an adjacent room.

PELE uses a dynamic approach to make the handoff decision, i.e., switching between the two localization modes. The handheld's accelerometer is leveraged to detect motionlessness, which is a good indicator for the handheld being left behind. At this point, the location of the user is the same as the handheld room, and the localization process enters the *localization neutral zone*. Using the map data, the distance between the handheld's absolute location (based on standalone localization) and the closest wall is determined. This distance determines the dynamic handoff threshold. Depending on the RSS of Bluetooth, the distance to the wearable is estimated. Once the user crosses the handoff threshold distance, the *joint* mode is triggered.

4.2 Sensor module

The sensor module in the wearable receives a trigger from the handoff manager when the switching to the joint mode takes place. The handheld sends a message to the wearable over the Bluetooth connection to indicate the switching. Only at this point, the accelerometer and the magnetometer units are activated on the wearable. The sampling rate for the accelerometer is set to 20 Hz as this is the

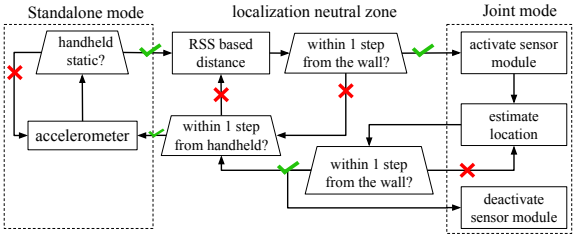

Figure 5: Switching between the two localization modes by the handoff manager.

minimum required rate to identify frequencies in human locomotion, including steps, accurately [1]. However, the magnetometer is not sampled at a fixed frequency. Rather it is sampled in an event driven manner: every time when a step is detected by the motion module. The details of step detection by the motion module based on accelerometer data are discussed in Section 4.3. Additionally, the Bluetooth RSS is measured on the wearable to calculate the distance from the handheld.

4.3 Motion module

The motion module receives the data from the sensor module, processes it, and provides three pieces of information – (i) the number of steps detection, (ii) the heading direction of the user, and (iii) the distance between the user and the handheld.

Step detection. Marschollek *et al.* [13] provides a comparison among various accelerometer-based step detection techniques. Results show that waist-worn or ankle-worn devices performs significantly better than the wrist-worn device. Wearable manufacturers achieve robust step detection for wrist-worn devices by using sophisticated and proprietary algorithms. As step detection is not the primary focus of this work, we use a simple step detection mechanism. Each time the accelerometer data is sampled, total acceleration is calculated by computing the magnitude from three axis components. If this magnitude crosses a predefined threshold, it is considered as a step. Once the step is detected, the sampling is paused for a small duration roughly equalling the duration of an average step. This avoid multiple (false) step detection within the same step period.

Heading detection. Depending on the type of wearable, robustness in the heading detection can vary. While orientation of a waist-worn wearable generally does not change relative to the true walking direction, head-mounted wearables will clearly follow the viewing direction. As we assume a wrist-worn wearable, we make the assumption that the arm swing in human locomotion is parallel to the true walking direction. A magnetometer alone cannot detect heading under these circumstances due to different tilt angles of the wearable throughout the swing. Hence, a tilt compensated compass using magnetometer and accelerometer is necessary. For this, we acquire an accelerometer sample, which gives an indication of the gravity vector $\boldsymbol{a} = \begin{bmatrix} a_x & a_y & a_z \end{bmatrix}^T$, and a magnetometer sample, a vector pointing to magnetic north $\boldsymbol{e} = \begin{bmatrix} e_x & e_y & e_z \end{bmatrix}^T$. By using their cross-product, we compute a third vector $\boldsymbol{h}$ perpendicular to both, $\boldsymbol{a}$ and $\boldsymbol{e}$.

As the accelerometer and the magnetometer vectors are generally not perpendicular due to earth's spherical shape and location

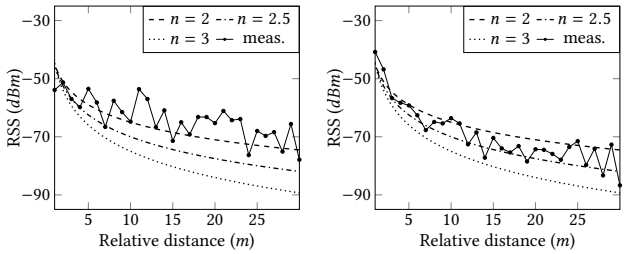

(a) corridor acting as waveguide (b) obstructing walls

Figure 6: Relative distance of devices and corresponding RSS.

dependent inclination, we compute vector $\hat{\boldsymbol{m}} = \hat{\boldsymbol{a}} \times \hat{\boldsymbol{h}}$ as a better representation of magnetic north. This vector $\hat{\boldsymbol{m}}$ is already a unit vector, because $\hat{\boldsymbol{a}}$ and $\hat{\boldsymbol{h}}$ are. Using the sign of the vector components h_y and m_y, we can compute the heading angle using trigonometric principles.

Distance estimation. Though RSS-based distance estimation can be erroneous, especially in the indoor environments, we use it as a secondary mechanism. As the dead-reckoning is also subject to error, the RSS-based distance estimation is used to calibrate during the localization process. How these two error-prone technique complement each other to establish an accurate location information is described in Section 4.4.

As the devices are paired using Bluetooth, the RSS, which represents the relationship between transmission and received power, can give an estimate of their distance. Eq. 1 presents a common approach towards distance estimation for the received signal strength S in dBm [14].

$$S = -10\eta \log_{10} d + A. \tag{1}$$

Here, η is the propagation path-loss exponent ($\eta = 2$ for free space), d is the distance between the sender and the receiver in meters and A is the received signal strength at one meter of distance.

To decide an appropriate path loss exponent, we measured RSS with increasing distance between the handheld and the wearable. When the devices were in line-of-sight in a long corridor, the resulting path loss exponent is at times less than 2 (Fig. 6a). The reason behind this is that a long corridor resembles a tunnel, which may act as a wave guide, providing a stronger signal at a relatively longer distance [15]. The measurements confirm the observations made in the work of [4] as RSS being rather unreliable. Furthermore, it has been found empirically that a wall reduces the signal power by approximately 3 dBm (depending on wall type and construction) [7]. In subsequent measurements with walls and furniture in the path a stronger down-trend of the resulting signal was observed, indicating a higher signal attenuation. In such cases, a better approximation of the loss exponent is $\eta = 2.5$ or higher (Fig. 6b).

In order to cope with the deviation, a low-pass filter was implemented, which cancels out high frequency noise. Note that we are smoothing the distance d rather than the RSS value directly. The reason is that the RSS being in a logarithmic relationship to the distance. Therefore, smoothing the RSS directly may result in changing responsiveness of the system at different distances between handheld and wearable.

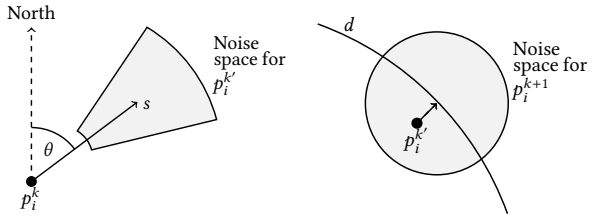

(a) dead-reckoning based relocation (b) device-distance based relocation

Figure 7: Noise added during particle relocation to catalyze convergence.

4.4 Location estimator

To estimate the location of the user, PELE integrates the information received from the motion module with the map data using a particle filter. The particle distribution is initiated when the *joint* mode is triggered by the handoff manager. As the user walks further, the particle positions are updated using two sequential mechanisms: first, dead-reckoning, second, distance-based calibration. As dead-reckoning is prone to cumulative errors, the RSS-based distance is used to rectify this error.

To expedite the particle convergence initial particle distribution is done judiciously. As mentioned in Section 4.1, the handoff takes place when the user moves beyond the threshold distance from the handheld; but still resides in the same room. Considering the *handheld room* as the initial location, all the particles are distributed in this room. However, if particles are distributed all over the room, they may form multiple clusters if there are multiple exits from this handheld room. To tackle this issue, the particles are projected in a arc with mean being the heading direction θ plus the heading noise introduced into the system.

Similar to the work in [16], each particle is represented using a 2D coordinate on the floor map, where particle i at step k has coordinate (x_i^k, y_i^k). If the user is heading at an angle of θ, and his/her stride length is s, then, each particles' location is updated with each step as follows.

$$x_i^{k'} = x_i^k + (s + l_i^k)\cos(a_i^k + \theta), \tag{2}$$

$$y_i^{k'} = y_i^k + (s + l_i^k)\sin(a_i^k + \theta). \tag{3}$$

Here, l_i^k and a_i^k are the stride length noise and heading noise respectively, which are deliberately added to the system to account for unreliable RSS as well as heading estimate. As a result, the particles are relocated to any location within a determined region as shown in Fig. 7a. This noise is also added to catalyze the particle convergence and improve recoverability from errors. The noise values are chosen from the uniform distributions where s and θ are the mean of the distributions, respectively. The range of the distributions are selected experimentally and discussed in Section 5. Next, we perform device distance-based calibration, which can eliminate the integration error caused by dead-reckoning. It projects particles into a location corresponding to the distance d between the devices (Fig. 7b). The value of d is calculated by the distance estimator based on the RSS value received at the wearable. To do so, we transform the coordinate $(x_i^{k'}, y_i^{k'})$ of a particle $p_i^{k'}$ from the map coordinate system to a coordinate system centered at the handheld's location

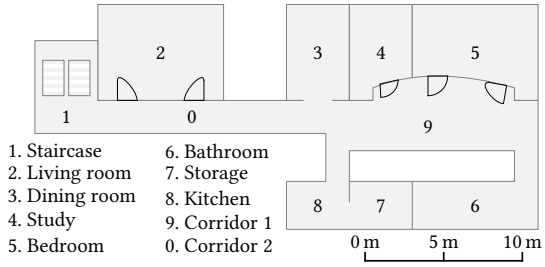

Figure 8: Floor plan of the indoor environment that is considered for calibration and testing of the proposed system.

(x_0, y_0) and compute the length of the resulting vector $\boldsymbol{u_i}$ as,

$$\boldsymbol{u_i} = (x_i^{k'} - x_0, y_i^{k'} - y_0). \tag{4}$$

This vector is scaled to have length equal to the radius of the distance sphere, resulting in $\boldsymbol{v_i}$,

$$\boldsymbol{v_i} = \frac{d}{|\boldsymbol{u_i}|}\boldsymbol{u_i} \tag{5}$$

Finally, we scale the vector back to the map coordinate system to get the projection pointed to by the vector $\boldsymbol{w_i}$.

$$(x_i^{k+1}, y_i^{k+1}) = \boldsymbol{v_i} + (x_0, y_0) \tag{6}$$

As a last step, uniformly distributed noise is added by further relocating the particle p_i randomly within a spherical noise space with radius n around the projected point (Fig 7b). This accounts for the unreliable RSS value as well as diminishes the bias introduced by the projection of a particle.

The newly acquired location is then validated, i.e., whether it is outside the mapped area or if the line joining (x_i^k, y_i^k) and (x_i^{k+1}, y_i^{k+1}) intersects a wall on the map. In such cases, the particle is eliminated and resampled in a valid and randomly chosen particle's location at the previous step.

5 EVALUATION

In this section we present the performance evaluation of our system with respect to location accuracy, computational complexity and robustness of the localization process, and also the efficiency of the handoff mechanism. The evaluation has been performed in an indoor environment spanning about 320 m^2. Fig. 8 shows the floor plan of the area, where the area has 10 rooms. The central corridor including the staircase and two rooms has an end-to-end distance of about 30 meters. While Bluetooth can theoretically have a range of more than 100 m, the practical communication range is significantly less, especially in the indoor environment. However, the longest distance in our experimental area is within the communication range (20 m) of the wearable device.

5.1 Accuracy

As room-level accuracy is sufficient in most of the indoor living spaces, the primary target of PELE is to achieve such accuracy. First, it was tested whether the system is capable to determine the location and track the room-to-room movement of the user within the test environment. For this, the movement accuracies for a limited number of pairs of rooms is evaluated. Fig. 9 summarizes the results of this evaluation, which are average of 10 experiments

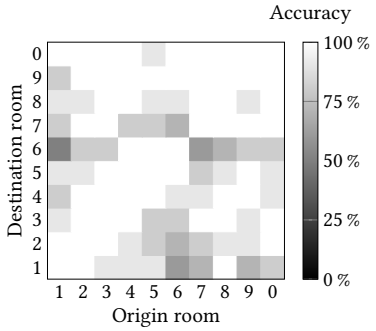

Figure 9: Confusion matrix of room transfer accuracy.

Table 1: Accuracy by room distance.

Room distance	Accuracy
<10 m	96.91 %
<20 m	93.54 %
<30 m	91.20 %

Table 2: Noise quantification.

Noise level	Stride length	Heading
0 %	s	θ
25 %	$s \pm 0.25s$	$\theta \pm 11.25°$
50 %	$s \pm 0.5s$	$\theta \pm 22.5°$
75 %	$s \pm 0.75s$	$\theta \pm 33.75°$
100 %	$s \pm s$	$\theta \pm 45°$

for every pair of rooms. Though, most of the room combinations (origin and destination room) show accurate location estimation, there are a few cases where the accuracy is below average (generally involving rooms 1, 6, and 7).

Classifying movement accuracy contextually by absolute room distance reveals that localization accuracy decreases with increasing distance from the room where the handheld currently is, say, *handheld room* (Table 1). As RSS-based distance estimate gets hampered with larger distance, the localization accuracy also decreases at far ends of the indoor environment. In addition, the lower accuracy involving rooms 6 and 7 can be explained by the position and access to the rooms. While the width of the walls in between rooms 2 through 5 are almost same (about 10 cm), rooms 6 and 7 can only be accessed through small corridors, that are heavily reinforced with concrete. Hence, the un-uniform density of an indoor environment causes low accuracy in our localization system.

Next, we experimented with 10 people with varying age, height, and gender. The users were asked to transfer randomly between rooms considering, two different handheld locations for each of them. The location of the handheld, i.e., the initial location of the user is determined using the *standalone mode* and not included in this evaluation.

The experiments are started after the handheld is kept on a table. At this point, the system enters the *localization neutral zone*. As the user moves away from the handheld gradually, the handoff takes place and the localization in *joint mode* starts. As mentioned earlier, the handoff takes place based on the dynamic handoff threshold distance, which is decided based on the distance between the nearest wall and the handheld. As the user moves from room to room, the location is also updated accordingly. Note that the origin room is not kept fixed. Based on a total of 350 room transfers, we found the localization accuracy of 90.31 % in PELE.

5.2 Particle filter optimization

The computing load is distributed over the handheld and the wearable, however, it is not even. Both the devices are limited in processing capability and power supply, with the handheld being generally more capable. Therefore, the particle filter has been implemented to run on the handheld, where the wearable provides the required information to update the particles based on the sensor data. However, to avoid unnecessary processing and memory consumption, the particle filter can be optimized by limiting the number of particles. On the other hand, more ambiguity can be rectified with an abundant number of particles. Thus, there is a clear trade-off between the number of particles and accuracy.

However, the noise is added to the system first, while evaluating the particle relocation (see Fig. 7) with an abundant number of particles. The various noise levels that are used in the experiments are quantized in Table 2. As mentioned earlier, stride length noise and heading noise for the dead-reckoning approach is introduced. The distance noise n has been predetermined to be $3s$, where s is stride length. This measure is retrieved from the floor plan and can slightly vary for different indoor environments, depending on the size of rooms and number of room entrances. The distance noise resembles the radius of a sphere, which barely fits in the smallest room on the floor plan (Room 7). It distributes the particles as much as possible, without allowing too much leakage to the adjacent room, in this example, Room 8. The noise added is uniformly distributed. The use of a specific probability distribution is deliberately avoided, to maintain the independence of the particles from one another, and thus avoiding artificially forced particle convergence. The noise is chosen in relation to a person's stride length s. Average stride length has been found to be about 75 cm, though it mostly varies based on the height of the user.

Fig. 10a summarizes the localization accuracy against various noise levels. Though, there is no observable clear trend, the performance seems to reach the peak around the noise level of 75 %. After this, the performance seems to decrease with higher noise levels. This could be caused by the enlarged space due to noise for the heading angle getting, as well as stride length varying too drastically between particles. Data suggests that it cannot be concluded with certainty, that the noise levels below 75 % are not entirely unsuitable. However, it was decided to use said noise level as default for all the evaluations.

When testing accuracy of the localization process with respect to the number of particles it could be concluded from Fig. 10b that at least 300 particles are necessary to provide good accuracy. This value may vary depending on the factors such as the average room size of the indoor environment and the number of rooms and also distance between entrances of rooms. However, for all experiments, a number of 300 particles ware adopted. This is selected using multiple experiments with varying number of particles. We found 300 particles as the minimum number to find room level accuracy, which also decreases the number of computations on the handheld.

5.3 Bluetooth communication

As communication incurs significant energy consumption, a less frequent packet transmission would be energy efficient. However, it may severely impact the localization process. To study this impact,

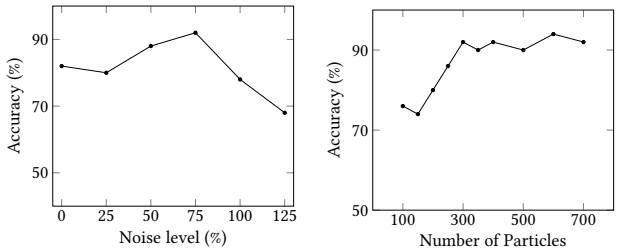

(a) optimizing amount of noise **(b) optimizing amount of particles**

Figure 10: Particle filter optimization.

Table 3: Accuracy v/s communication.

Packets missed	Accuracy
0	91.20 %
1	74 %
2	66 %
3	<50 %

Table 4: Energy consumption by various system components.

Activity	Current
Bluetooth connection	10 μA
Handheld accelerometer	3 μA
Wearable accelerometer	3 μA
Wearable magnetometer	100 μA
Transmit packet	2 μA

we sent packets with larger intervals, i.e., instead of sending packets at every step detection, a packet is sent every second, third and fourth step. This provides incomplete information. Though the system continued to perform reasonably well for missing every second step in the corridor (Rooms 0 and 9), it often misses the smaller room. The accuracy further degrades with more missing steps as it is summarized in Table 3.

The results signify that even if steps missed once in a while, it would not introduce an unrecoverable error. In fact, the RSS based calibration aids such scenarios when packets are lost or steps go undetected, as it calibrates the particles onto the most recent distance. Decreasing communication rate by default is not advised as it decreases accuracy accordingly.

5.4 Hand-off

Switching from *standalone mode* to *joint mode* is crucial, because on handoff, the particles are projected into the heading direction of the user. If projection happens in the wrong direction with respect to a specific room where handheld is with multiple exits, where recovery will not happen unless the user returns to the room having the handheld. The evaluation of handoff mechanism has been evaluated and shown in Fig. 9. It uses the transfer accuracy through an exit from the handheld room to an adjacent room. This transfer was successful in 97 % of the cases. Handoff accuracy directly contributes to the overall accuracy within 10 m of range from the origin room.

Averaged component power consumption of the hardware configuration is summarized in Table. 4. It is important to note that maintaining the Bluetooth connection also enables gathering RSS values. Handoff mode offers possibilities to save energy, considering that the sensors are significantly more energy demanding than the energy necessary to maintain a Bluetooth connection.

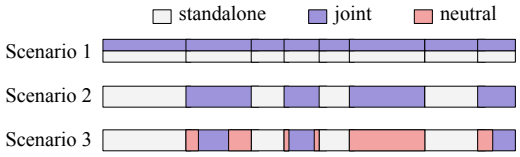

Figure 11: Handoff evaluation using different scenarios.

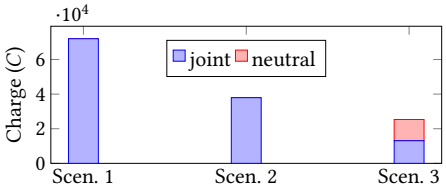

Figure 12: Energy consumption of wearable.

To evaluate the room for energy saving further, Fig. 11 presents three scenarios in which a user switches between the *standalone*, *joint* and *neutral* localization modes. Each time *standalone mode* makes up 47.3 % of the overall duration of the scenario and *joint mode* makes up 52.7 %. The absolute duration of the scenario is one hour. In Scenario 1, both these modes are active continuously. In Scenario 2, a handoff takes place when mode changes. In Scenario 3, the handoff is complemented by the *neutral mode*, which is during the time between the other two modes. That means 34 % of the entire duration is in neutral mode, which corresponds to 65.5 % of the time *joint mode* should have been active. The results in Fig. 12 suggest that there is a benefit due to the handoff mechanism. If the wearable would be active throughout as in Scenario 1, the energy would deplete about twice as fast as with separate modes for *joint mode* and *standalone mode* as in Scenario 2. Scenario 3 shows the benefits of the handoff mechanism and the *localization neutral* mode, which decreases energy consumed even further compared to Scenario 2.

6 CONCLUSION

Indoor localization is an important enabler for pervasive IoT services. As handhelds are generally not carried continuously in non-public indoor environments, the necessity for a wearable-based localization system arises to enable smart indoor applications. Existing methods are heavily tuned for the handhelds with respect to requirements of sensors, processing capability, and energy. This work presents a distributed system, called **PE**rvasive **L**ocalization **E**ngine (PELE), that jointly uses a handheld and a wearable device. It uses two modes of operation. In *standalone mode* only the handheld is used for localization. Once the user leaves the handheld behind, the *joint mode* is triggered, where the user is localized relative to the handheld using a common BLE connection. PELE uses a particle filter that fuses information from dead-reckoning and distance-based calibration. Additionally, the handoff mechanism of PELE optimizes the sensing and processing on the devices. The system achieves a localization accuracy of 90.3 %, and handoff reliability of 97 % along with energy savings up to 50%.

REFERENCES

[1] Carlijn VC Bouten, Karel TM Koekkoek, Maarten Verduin, Rens Kodde, and Jan D Janssen. 1997. A triaxial accelerometer and portable data processing unit for the assessment of daily physical activity. *IEEE Transactions on Biomedical Engineering* 44, 3 (1997), 136–147.

[2] Luca Calderoni, Matteo Ferrara, Annalisa Franco, and Dario Maio. 2015. Indoor localization in a hospital environment using Random Forest classifiers. *Expert Systems with Applications* 42, 1 (2015), 125–134.

[3] Digi-Key. 2016. Digi-Key Electronics. (2016). Available: http://digikey.com [Accessed Sep. 23, 2016].

[4] Eiman Elnahrawy, Xiaoyan Li, and Richard P Martin. 2004. The limits of localization using signal strength: A comparative study. In *First Conference on Sensor and Ad Hoc Communications and Networks (SECON)*. IEEE, 406–414.

[5] João Sena Esteves, Adriano Carvalho, and Carlos Couto. 2003. Generalized geometric triangulation algorithm for mobile robot absolute self-localization. In *Industrial Electronics, ISIE'03. International Symposium on*, Vol. 1. IEEE, 346–351.

[6] Mouser Europe. 2016. Mouser Electronics. (2016). Available: http://eu.mouser.com [Accessed Sep. 23, 2016].

[7] Xu Huang, Mark Barralet, and Dharmendra Sharma. 2009. Accuracy of location identification with antenna polarization on RSSI. In *Proceedings of the International MultiConference of Engineers and Computer Scientists*, Vol. 1. Citeseer.

[8] Antonio R Jimenez, Fernando Seco, Carlos Prieto, and Jorge Guevara. 2009. A comparison of pedestrian dead-reckoning algorithms using a low-cost MEMS IMU. In *Intelligent Signal Processing, International Symposium on*. IEEE, 37–42.

[9] Wonho Kang and Youngnam Han. 2015. SmartPDR: Smartphone-based pedestrian dead reckoning for indoor localization. *IEEE Sensors journal* 15, 5 (2015), 2906–2916.

[10] Swarun Kumar, Stephanie Gil, Dina Katabi, and Daniela Rus. 2014. Accurate indoor localization with zero start-up cost. In *Proceedings of the 20th annual international conference on Mobile computing and networking*. ACM, 483–494.

[11] Hui Liu, Houshang Darabi, Pat Banerjee, and Jing Liu. 2007. Survey of wireless indoor positioning techniques and systems. *IEEE Transactions on Systems, Man, and Cybernetics, Part C (Applications and Reviews)* 37, 6 (2007), 1067–1080.

[12] Dimitrios Lymberopoulos, Jie Liu, Xue Yang, Romit Roy Choudhury, Vlado Handziski, and Souvik Sen. 2015. A realistic evaluation and comparison of indoor location technologies: Experiences and lessons learned. In *International conference on Information processing in sensor networks (IPSN)*. ACM.

[13] Michael Marschollek, Mehmet Goevercin, Klaus-Hendrik Wolf, Bianying Song, Matthias Gietzelt, Reinhold Haux, and Elisabeth Steinhagen-Thiessen. 2008. A performance comparison of accelerometry-based step detection algorithms on a large, non-laboratory sample of healthy and mobility-impaired persons. In *IEEE International Conference on Engineering in Medicine and Biology Society*. 1319–1322.

[14] O Oguejiofor, V Okorogu, A Adewale, and B Osuesu. 2013. Outdoor localization system using RSSI measurement of wireless sensor network. *International Journal of Innovative Technology and Exploring Engineering* 2, 2 (2013), 1–6.

[15] Jane Radatz. 1997. *The IEEE standard dictionary of electrical and electronics terms*. IEEE Standards Office.

[16] Anshul Rai, Krishna Kant Chintalapudi, Venkata N Padmanabhan, and Rijurekha Sen. 2012. Zee: zero-effort crowdsourcing for indoor localization. In *International conference on Mobile computing and networking*. ACM, 293–304.

[17] Milan D Redžić, Conor Brennan, and Noel E O'Connor. 2014. SEAMLOC: Seamless Indoor Localization Based on Reduced Number of Calibration Points. *IEEE Transactions on Mobile Computing* 13, 6 (2014), 1326–1337.

[18] Chayan Sarkar, SN Akshay Uttama Nambi, R Venkatesha Prasad, and Abdur Rahim. 2014. A scalable distributed architecture towards unifying IoT applications. In *Internet of Things (WF-IoT), 2014 IEEE World Forum on*. IEEE, 508–513.

[19] Chayan Sarkar, Vijay S Rao, R Venkatesha Prasad, Abdur Rahim, and Ignas Niemegeers. 2012. A distributed model for approximate service provisioning in internet of things. In *Proceedings of the 2012 international workshop on Self-aware internet of things*. ACM, 31–36.

[20] Chayan Sarkar, Akshay Uttama Nambi SN, and R Venkatesha Prasad. 2016. iLTC: Achieving Individual Comfort in Shared Spaces. In *Proceedings of the International Conference on Embedded Wireless Systems and Networks (EWSN)*. ACM.

[21] Mitilineos A Stelios, Argyreas D Nick, Makri T Effie, Kyriazanos M Dimitris, and Stelios CA Thomopoulos. 2008. An indoor localization platform for ambient assisted living using UWB. In *Proceedings of the 6th international conference on advances in mobile computing and multimedia*. ACM, 178–182.

[22] Attila Török, András Nagy, László Kováts, and Péter Pach. 2014. Drear-towards infrastructure-free indoor localization via dead-reckoning enhanced with activity recognition. In *2014 Eighth International Conference on Next Generation Mobile Apps, Services and Technologies*. IEEE, 106–111.

[23] He Wang, Souvik Sen, Ahmed Elgohary, Moustafa Farid, Moustafa Youssef, and Romit Roy Choudhury. 2012. No need to war-drive: unsupervised indoor localization. In *Proceedings of the 10th international conference on Mobile systems, applications, and services*. ACM, 197–210.

[24] Viveca Woods and Rob Van der Meulen. 2016. Gartner Says Worldwide Wearable Devices Sales to Grow 18.4 Percent in 2016. (2016). Available: http://gartner.com/ [Accessed Sep. 23, 2016].

[25] EGB Workgroup. 2009. *Buildings and their impact on the environment: a statistical summary*. Technical Report. US Environmental Protection Agency.